Closure magnetization configuration around a single hole in a magnetic film

G. Rodríguez-Rodríguez,[1,2] H. Rubio,[2] M. Vélez,[2] A. Pérez-Junquera,[2] J. V. Anguita,[3] J. I. Martín,[2,*] and J. M. Alameda[2]
[1]*Instituto Nacional del Carbon (INCAR), CSIC, c/Francisco Pintado Fe 26, 33011 Oviedo, Spain*
[2]*Departamento de Física, Universidad de Oviedo-CINN, 33007 Oviedo, Spain*
[3]*Instituto de Microlectrónica de Madrid (CNM-CSIC), Tres Cantos, 28760 Madrid, Spain*
(Received 16 July 2008; revised manuscript received 26 September 2008; published 17 November 2008)

The basic problem of a single hole in a magnetic film with uniaxial anisotropy has been analyzed in detail by magnetic force microscopy, micromagnetic simulations, and an analytical model. The closure magnetization configuration can be described by two $-1/2$ half vortices located at the hole edge along the easy anisotropy axis and confined within a distance L that is determined by the minimization of magnetostatic and anisotropy energies constrained by the magnetic charge conservation within the system.

DOI: 10.1103/PhysRevB.78.174417 PACS number(s): 75.60.Ej, 75.60.Ch, 74.25.Qt

I. INTRODUCTION

The study of magnetic nanostructures either in the shape of thin-film magnetic nanoelements or of continuous patterned magnetic films has deserved increased attention in recent years[1] due to their possible applications in the field of high-density magnetic recording.[2] One common feature in many of these magnetic nanostructures, such as magnetic nanorings,[3–6] thin films patterned with arrays of antidots,[7–12] or magnetic disks with controlled defects,[13] is the existence of nonmagnetic holes within the magnetic material. Most of the attention has been devoted to the analysis of the different magnetic configurations corresponding to each different kind of structure, such as the transitions between in-plane axial and vortex states in nanorings,[14] or the different kinds of periodic closure domain structures in magnetic films with antidots.[15] Recently, a general picture of the physics of thin-film nanorings and other flat nanoelements has been given in terms of single topological defects in the limit of negligible anisotropy.[16] However, up to now, the simplest though fundamental problem of a continuous magnetic film with a single nonmagnetic hole has received little attention.

The corresponding problem in three dimensions (3D), i.e., that of a nonmagnetic inclusion in a bulk magnetic material, has long been studied[17–19] and has provided the basis for coercivity models in soft magnetic materials, in which the inclusions act as domain-wall pinning centers. The balance between the magnetostatic energy associated with the poles that appear at the edges of the inclusion and domain-wall energy results in the formation of a typical closure domain structure consisting of a pair of blade-shaped domains centered at the hole.[20] The observations of the magnetic configuration around holes in thin films[21–24] reveal a very different behavior that is related with the different character of magnetostatic interactions in bulk materials and in thin films (in a similar way as there is a change in the preferred domain-wall structure from Bloch to Néel walls as the film thickness is decreased). However, to our knowledge, this problem has only been discussed in a qualitative way[21] in terms of a magnetization pattern that curves around the hole in order to avoid the magnetic poles in its surface, but it has not been analyzed in detail in a quantitative manner. A two-dimensional (2D) model used to obtain the domain configuration in soft ferromagnetic films was developed by van den Berg[25] using the method of characteristics, and it was extended by Bryant and Suhl[26] to the case of a sufficiently weak in-plane applied field through an electrostatic analogy. However these models are restricted to finite and simply connected magnetic film elements, that is, without holes.[27,28]

In this work, a characterization of the closure structure around a patterned hole in a soft amorphous magnetic film has been performed by magnetic force microscopy (MFM) and micromagnetic simulations using the OOMMF code.[29] The results are analyzed in terms of a simple theoretical model based both in the principle of pole avoidance solving the Laplace equation for the magnetization lines in 2D and in the Gauss theorem so that the analysis can be extended to multiply connected and infinite films. This allows one to understand the dependence of the confinement distance of the singularities created by the hole on the different material parameters.

II. EXPERIMENT

Amorphous $Co_{86}Zr_{14}$ 40-nm-thick magnetic films have been grown on Si substrates by cosputtering as reported elsewhere.[30] The films have a well-defined uniaxial anisotropy with typical easy anisotropy fields $H_K=4$ kA/m. Saturation magnetization M_s for this alloy composition is $M_s=4\times10^5$ A/m so that the anisotropy energy can be calculated as $K=\mu_0 M_s H_K/2=1\times10^3$ J/m^3. The films have been patterned with an array of nonmagnetic holes by a combination of electron-beam (e-beam) lithography and Ar^+ etching processes.[30] The defined holes are circles with 2 μm diameter and are arranged in a 20×20 μm^2 square cell. Interhole distances are much larger than hole size so that the array can be considered effectively in the diluted limit,[24] in which the holes act as isolated inclusions and no periodic domain-wall pattern is developed in the array. The magnetic configuration around each hole has been characterized using a Nanotec™ force microscopy system with Nanosensors™ point probe plus magnetic force microscopy-reflex coating (PPP-MFMR) commercial tips. The measurements were performed in a dynamical retrace mode in which the topographic profile of a single line is scanned first, and then, this line is repeated at a retrace height (typically between 20 and

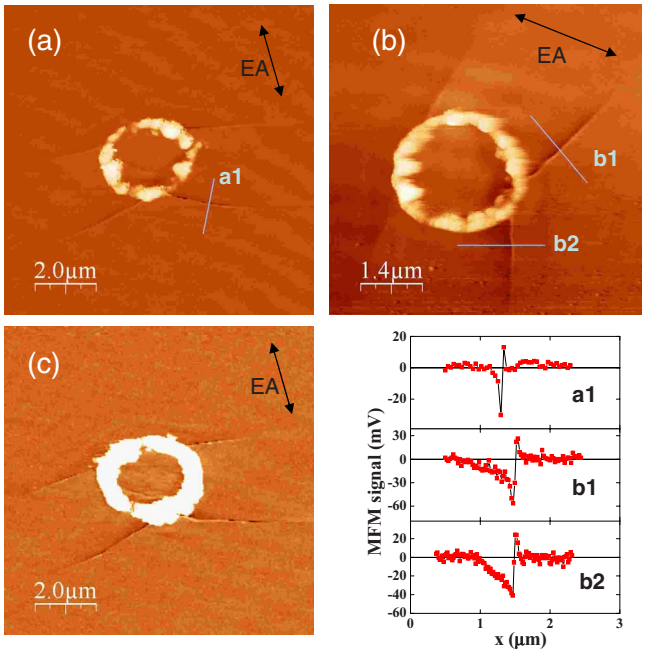

FIG. 1. (Color online) [(a)–(c)] MFM images of the domain configuration around several patterned holes in a Co-Zr thin film. Double arrows indicate the uniaxial anisotropy easy axis in each image. (a1), (b1), and (b2) MFM signal along the indicated profiles taken across the different walls [indicated by solid lines in panels (a) and (b)].

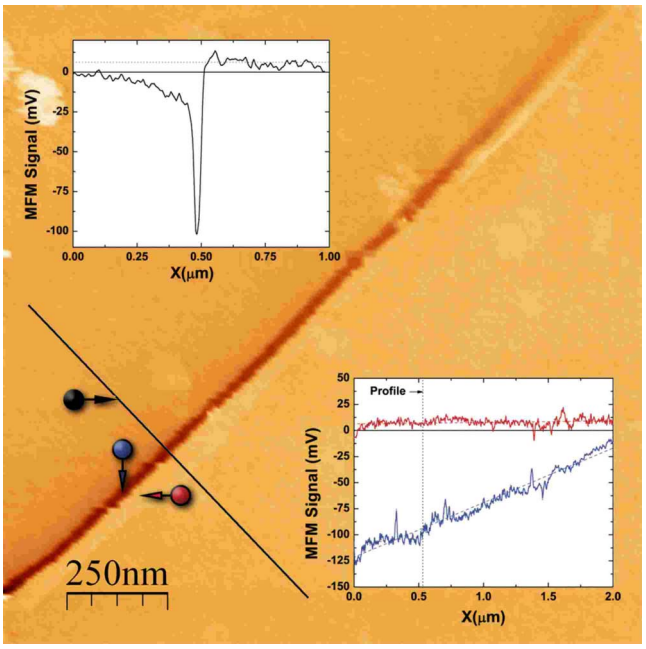

FIG. 2. (Color online) MFM image of one of the walls emanating from the patterned hole. Top inset: MFM signal along a profile taken across the wall (indicated by solid line). Bottom inset: evolution along the wall of the MFM signal at the maximum and minimum contrast points (dark and clear lines defining the wall).

150 nm higher than topography scan) following the first scanned profile. The samples were saturated at 0.27 T along the easy axis prior to the MFM characterization that was, then, performed at zero external field in the remanent state.

III. MFM CHARACTERIZATION

Figure 1 shows several MFM images of the area around patterned holes taken at 20 nm retrace height. In all the studied holes a very similar closure magnetization configuration is observed and is in good agreement with previous studies of holes in permalloy films:[21,23] it is symmetric around the film anisotropy axis and consists of two pairs of domain walls that emanate from opposite sides of the hole and extend for about 3 μm inside the film. The domain walls are curved close to the hole and become approximately perpendicular to the easy axis direction before they disappear inside the film. The white rim that appears around the holes is a remnant of the topographic contrast at the hole edge. The differences between the wall configurations at opposite sides of the hole can be attributed to tip-sample interactions, as they disappear for longer retrace distances at the expense of a lower resolution.[31] The walls present a dipolar contrast, which is more evident in the pairs that emanate from the bottom side of the holes, characterized by two parallel dark-clear lines. Even though an unequivocal determination of the wall structure cannot be made from MFM signal, this kind of images is typical of Néel walls[32] with the dark-clear contrast lines corresponding to the magnetic charges located at the core of the wall. This is reasonable since the critical thickness for the stability of Néel walls in this material can be estimated as[24,33] 60 nm which is larger than the film thickness of 40 nm. Line profiles of the MFM signal taken at different positions along the walls (panels a1, b1, and b2 in Fig. 1) show an asymmetry between the amplitude of the positive and negative contrast peaks with the negative contrast extending over a larger distance away from the wall.

The wall structure can be seen in more detail in Fig. 2, which is a magnified view of the end portion of one of these walls with the distance from the hole edge increasing from left to right. It can be seen again that the wall is characterized by a pair of dark-clear contrast lines that run parallel along the diagonal of the image until they fade away close to the top-left corner of Fig. 2, i.e., as the distance from the hole is increased. The width of the wall core can be estimated from the distance from the maximum and minimum contrast points in the profile shown in the inset at the top of Fig. 2. It is constant along the wall and takes a value of around 50 nm. This is in reasonable agreement with the estimate for the width of the Néel wall core in $Co_{86}Zr_{14}$: $W_{core} = 2(2A/\mu_0 M_s^2)^{1/2} = 20$ nm, calculated using a value for the exchange constant $A = 1 \times 10^{-11}$ J/m that is typical of $3d$ magnetic materials, taking into account that the experimental value is always broadened due to the convolution with the tip stray field distribution. The inset at the bottom of Fig. 2 shows the evolution along the domain wall of the maximum and minimum contrast points. It can be seen that as the distance from the hole edge increases the negative value corresponding to the dark contrast line progressively decreases, whereas the positive value of the clear contrast line stays constant. There are several possible sources of an asymmetric MFM contrast from a Néel wall:[34] disturbances by the tip

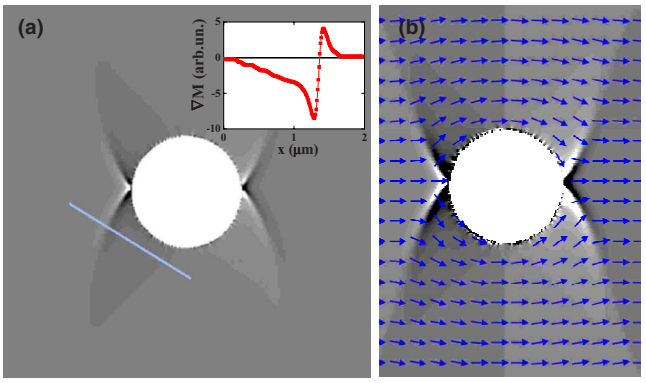

FIG. 3. (Color online) OOMMF simulations of the magnetic configuration around a hole in a Co-Zr magnetic film. (a) Map of the magnetization divergence around the hole. Inset shows the divergence profile taken across one of the walls (solid line) revealing an asymmetric charge configuration. (b) Same as in (a) but with an enhanced contrast by a factor of 3. Arrows indicate the direction of the local magnetization.

stray field, the existence inside the film of an asymmetric Néel wall or asymmetric Bloch wall with a Néel cap on the surface,[28] and/or a net magnetic charge localized at the wall core (due to a net component of the magnetization difference at both sides of the wall perpendicular to the wall). Finally, the progressive fading away of the wall contrast can be attributed to a decrease in the wall angle that, correspondingly, decreases the magnetic charges located at the wall core.

IV. MICROMAGNETIC MODELING

Figure 3 shows the results of the micromagnetic simulation of a hole of radius $R=0.75$ μm in a $Co_{86}Zr_{14}$ film using the OOMMF code.[29] The grayscale corresponds to the magnetization divergence, i.e., with the density of magnetic charges, and the arrows indicate the local magnetization direction. It can be seen that the magnetization is essentially parallel to the easy axis direction in the regions at the left and at the right of the nonmagnetic hole and also far enough above and below it. In two regions close to the hole edge, the magnetization is seen to rotate around the hole in order to become parallel to its edge. Taking into account that MFM is mainly a charge mapping microscopy, a qualitative comparison may be made between the MFM images of Figs. 1 and 2 and the calculated divergence images of Fig. 3, even though simulations of tip-sample interactions would be needed for a quantitative comparison.[35] The main features that appear in the calculated divergence image of Fig. 3(a) are very similar to those in the MFM images: two pairs of Néel walls generated at each side of the hole at the singularity points where the magnetization domain rotating clockwise meets the magnetization domain with counterclockwise rotation sense. The wall angle decreases from almost 90° close to the hole edge to almost 0° at about 2 μm from the hole, where the wall contrast in the divergence pattern fades away.

The wall contrast is indeed much more intense on one side of the wall core than on the other, as can be seen in the profile taken across one of them that is depicted in the inset of Fig. 3(a). The negative divergence peak is twice larger than the positive one, and the negative charges extend for a longer distance away from the wall center. It is interesting to mention that these calculated walls are predominantly of Néel character with a maximum magnetization deviation out of the film plane of less than 1×10^{-4} rad at the wall core. Thus, the similarities with the profiles of the MFM signal across the walls shown in Figs. 1 and 2 confirm that an important source of the observed asymmetry is the net magnetic charge localized at the wall core. Finally, in Fig. 3(b), a divergence map with an enhanced contrast, it can be seen that a nonzero magnetic charge density appears in the regions of curved magnetization; it indicates that in this 2D problem, the magnetic charges that would have been located at the hole in the case of uniform magnetization are distributed in a relatively large area around the hole (that corresponds roughly to the Néel tails of the pairs of walls that emanate from the hole). This results in a mixture of positive and negatively charged regions around the hole that cannot be simply described in terms of a dipole approximation. It is also very different from the more widely studied case of a spherical cavity in a bulk magnetic material, in which the walls involved in the closure structure are of Bloch type, and the main effect of the blade-shaped closure domains is to distribute the magnetic charges in a larger area to reduce the magnetostatic energy but essentially keeping the dipolar character of the magnetic field created at the spherical cavity.[20]

This closure structure around a hole in a 2D film can be described in terms of elementary topological defects, in a similar way as it has been done for nanoring structures in the onion state,[16] as being composed of two $-1/2$ half vortices located at opposite sides of the nonmagnetic hole. This makes it a very stable structure since the two half vortices have the same topological charge and cannot annihilate with each other. A magnetization reversal process of this closure structure would simply take place by the two half vortices exchanging positions along the hole edge, as it is indeed observed in micromagnetic simulations of a Néel wall crossing across the hole. There are, however, important differences between the problem of a single hole in an infinite film with uniaxial anisotropy considered here and the case of magnetic Permalloy nanorings in which magnetocrystalline anisotropy is usually neglected. First, the presence of a significant uniaxial anisotropy breaks the degeneracy of the circular hole shape creating an energy minimum for the location of the half vortices along the uniaxial anisotropy axis, and second and more important, the anisotropy confines the perturbation induced by the half vortices to a limited region close to the hole of size L by favoring a parallel alignment of the magnetization to the easy axis in the regions far enough from the hole. The infinite character of the considered film also forbids the presence of vortex states around the hole. This confinement distance L appears as the characteristic length scale to discriminate between arrays of holes in a diluted or concentrated regime (i.e., between a set of isolated holes or a film with a periodic domain pattern joining the hole) and to determine the range of interactions between a nonmagnetic inclusion and a domain wall crossing the film upon magnetization reversal.

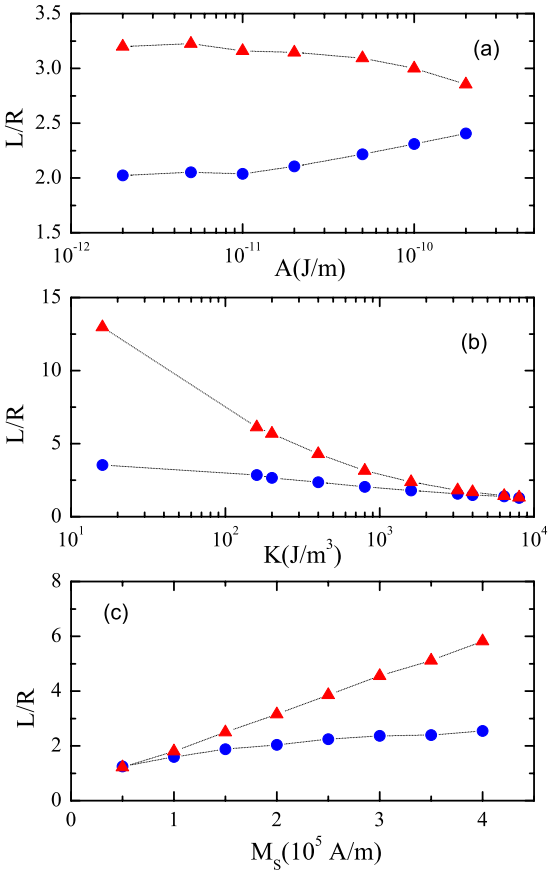

FIG. 4. (Color online) Size of the closure structure around a hole normalized by the hole radius R (a) as a function of exchange constant A ($K=8\times10^2$ J/m^3, $M_s=2\times10^5$ A/m); (b) as a function of uniaxial anisotropy K ($M_s=2\times10^5$ A/m, $A=1\times10^{-11}$ J/m); and (c) as a function of saturation magnetization M_s ($K=8\times10^2$ J/m^3, $A=1\times10^{-11}$ J/m): circles along the easy axis (L_x/R) and triangles perpendicular to the easy axis (L_y/R).

Figure 4 shows the size of the closure structure around the nonmagnetic hole L/R obtained from micromagnetic simulations as the point in which the magnetization deviation from the easy axis becomes smaller than 1° as a function of the different material parameters: exchange constant A [Fig. 4(a)], uniaxial anisotropy K [Fig. 4(b)], and saturation magnetization M_s [Fig. 4(c)]. The closure structure presents a clear anisotropic configuration with a larger extension perpendicular to the uniaxial easy axis (L_y/R) than along it (L_x/R). L_y/R is found to increase almost linearly as a function of M_s and to decrease smoothly as a function of material anisotropy. The ratio L_y/L_x varies between 1 and 4 in the studied parameter range and, in particular, for the material parameters corresponding to the used Co-Zr alloy, $L_y/L_x=2.3$, which is in good agreement with the experimental value obtained from the MFM characterization in Fig. 1, $L_y/L_x=2.5$. This geometrical factor shows opposite trends as a function of M_s and K so that the closure structures becomes more rectangular as its spatial extension becomes larger. This change in shape can be qualitatively attributed to the curved shape of the Néel walls that emanate from the singularity points: these walls would be straight lines at 45° to the hole edge in the absence of a confining uniaxial anisotropy[16] but curve away from the diagonals as they run further away from the hole edge, becoming almost perpendicular to the easy axis direction (and, thus, result in the observed rectangular shape of the closure structure). Finally, (L_y/R) is found to be only very weakly dependent on the exchange constant A in a wide parameter range. This indicates that the size of the closure structure is mainly determined by the balance between magnetostatic and anisotropy energies in the range of parameter values typical of $3d$ magnetic materials. Only for large values of the exchange constant ($A>1\times10^{-10}$ J/m) does L_y/R become dependent on A, and a qualitative change appears in the closure structure to a more square configuration, indicating a transition to a regime in which exchange energy overcomes the contribution of anisotropy energy.

V. ANALYTICAL MODEL

In order to study the underlying physical problem and get a better understanding of the interplay between the different factors that determine this confinement distance of the closure structure induced by the hole, an analytical model of this system can be made by considering an infinite 2D film with a circular hole of radius R. We denote by Ω and $\partial\Omega$ the space occupied by the ferromagnetic material and its boundary, respectively. The ferromagnetic film has a uniaxial anisotropy and due to the symmetry of the problem, we will choose the origin of coordinates at the center of the hole, the x axis in the direction of the easy axis of anisotropy, and the z axis perpendicular to the film plane. Any solution to the problem must scale with R; therefore, we denote by $\boldsymbol{\rho}=(\xi,\eta)=(\frac{x}{R},\frac{y}{R})$ and $(\rho,\theta)=(\frac{r}{R},\theta)$ the normalized Cartesian and polar coordinates, respectively, of a generic point. The numerical calculations in Sec. IV suggest that the relationship among exchange energy E_{ex}, anisotropy energy E_K, and magnetostatic energy E_m satisfies $E_{\text{ex}}\ll E_K\ll E_m$. Due to this relation, the possible magnetization configurations in the system will be mainly determined by the principle of pole avoidance, so that $\nabla\cdot\mathbf{M}$ must be as close to zero as possible. If $\nabla\cdot\mathbf{M}=0$, then $\mathbf{M}$ can be directly obtained from the vector potential $\mathbf{A}$ as $\mathbf{M}=\nabla\times\mathbf{A}$. In two dimensions, the magnetization $\mathbf{M}$ is restricted to the film plane and the vector potential is of the form $\mathbf{A}=(0,0,\psi)$. Then,

$$M_x=\frac{\partial\psi}{\partial y};\quad M_y=-\frac{\partial\psi}{\partial x},\tag{1}$$

so that $\mathbf{M}\cdot\nabla\psi=0$, i.e., $\mathbf{M}$ and $\nabla\psi$ are perpendicular. Thus the magnetization lines coincide with the contour lines of constant ψ.

From the principle of pole avoidance it follows that $\psi(\boldsymbol{\rho})$ must satisfy

$$\begin{cases}(\text{i})\nabla^2\psi=0 & \text{on } \Omega\\ (\text{ii})\dfrac{\partial\psi}{\partial\theta}=0 & \text{on } \rho=1\\ (\text{iii})\psi\sim M_s\rho\sin\theta & \text{as } \rho\to\infty\end{cases}.\tag{2}$$

The solution of the problem can be written as[36]

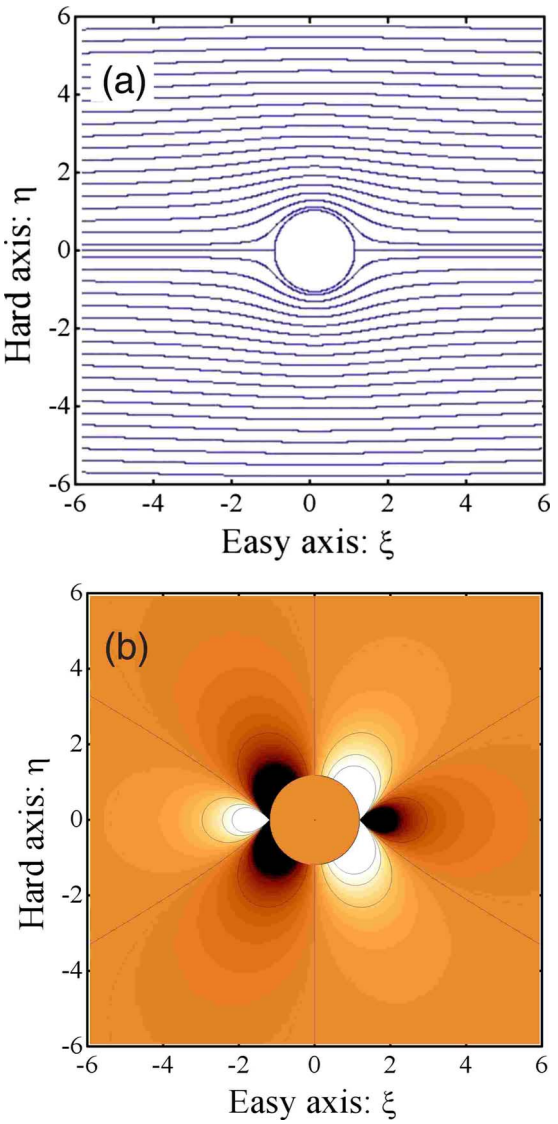

FIG. 5. (Color online) (a) Magnetization lines around a nonmagnetic hole derived from $\psi(\rho,\theta)$. (b) Magnetization divergence (i.e., magnetic charges) that is associated to the magnetization distribution in (a) upon imposing the condition of constant modulus $|\mathbf{M}|=M_s$ everywhere (note the mixture between positive and negative poles around the hole).

$$\psi(\rho,\theta) = M_s\left(\rho - \frac{1}{\rho}\right)\sin\,\theta. \tag{3}$$

This solution is equivalent to the one obtained from the overlap of a uniform field and a linear dipolar field in the opposite direction.[37,38] Figure 5(a) shows the magnetization lines derived from $\psi(\boldsymbol{\rho})$ given by Eq. (3). In this case there are no magnetic charges in the system since $\nabla\cdot\mathbf{M}=0$ everywhere. However, this result is not valid for a ferromagnetic material since it implies that the modulus of $\mathbf{M}$ changes from one point to another. In order to avoid a nonconstant $|\mathbf{M}|$, we assume that $\psi(\boldsymbol{\rho})$ describes the $\mathbf{m}=\mathbf{M}/M_s$ lines instead of the $\mathbf{M}$ lines. This normalization leads to the emergence of poles in the system. Figure 5(b) shows the divergences of magnetization corresponding to the $\mathbf{m}$ lines given in Fig. 5(a).

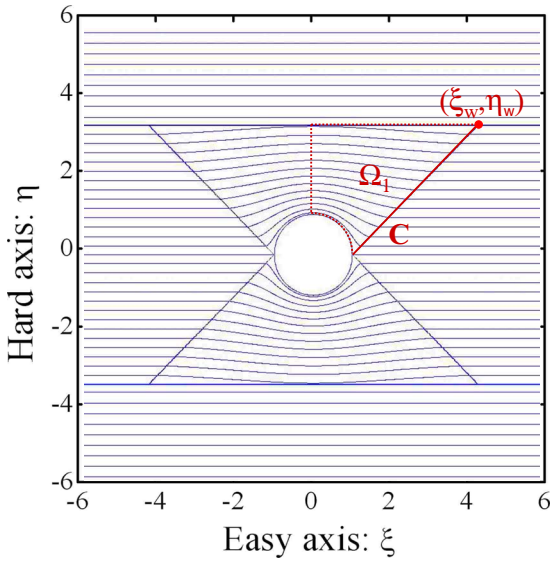

FIG. 6. (Color online) Sketch of the domain structure around the hole after introducing two pairs of straight domain walls emanating from the singularity points at $(\pm 1,0)$. Also indicated are the area Ω_1, the wall C, and the point (ξ_w,η_w) that define the area of integration for the application of the Gauss theorem.

These divergences are distributed symmetrically around the hole. In the close environment of the point (1,0) there exists a very high positive charge density and around $(-1,0)$ a very high negative charge density. Leaved regions of positive charges appear around the $+\xi$ axis and in the second and third quadrants with a low density that fades away from the hole. Besides, around the $-\xi$ axis and in the first and fourth quadrants other similar leaved regions of negative charges appear.

On the other hand, the $\psi=0$ line is made by the circumference of the hole plus two semistraight lines emerging from the points $\rho=1$ and $\theta=0,\pi$, respectively. The magnetization in these points seems to have two different directions simultaneously. Abolition of this ambiguity requires the introduction of a domain structure. Thus, from each of these points two domain walls should emanate. Or equivalently, each of these points becomes an edge defect with winding number $-1/2$. By introducing these four walls, the system will be divided into domains. The symmetry introduced by the easy axis and the boundary condition, which requires that the magnetization should be parallel to the easy axis when $\rho\gg 1$, suggests that the domain pattern is similar to that indicated in Fig. 6. This closure structure not only avoids the ambiguity at (1,0) and $(-1,0)$ but also reduces considerably the magnetostatic energy stored around the hole by eliminating the highly charged regions close to these points. In the limit of negligible exchange energy, as assumed here, the domain walls can be considered as infinitely thin lines over which the magnetization changes abruptly. The magnetization forms different angles on both sides of the walls; therefore, they are charged with a linear charge density λ.

These qualitative descriptions on the closure domain pattern must be converted into quantitative ones in order to determine the shape, length, and precise position of the walls. This can be obtained using the Gauss theorem. If a

saturating magnetic field is applied in the easy axis direction $\mathbf{e}=(1,0)$, free poles appear with density $\sigma=-M_s \cos\theta$ on the edges of the hole. When the applied field is reduced to zero, these charges will be distributed by the system. But due to the symmetry of the magnetization lines (which are parallel to $\mathbf{e}=(1,0)$ at all points on the ξ and η axes), the total charge in each quadrant must remain constant. This condition imposes a restriction on the position, shape, and length of the walls emanating from the $-1/2$ edge defects. Due to the symmetry of the system, we will examine only the first quadrant. Let C be the wall that emanates from the point (1,0) and ends at a point (ξ_w, η_w). Let Ω_1 be the area bounded by the edge of the hole, by the η axis, by the wall C, and by the straight line $\eta=\eta_w$. The direction of the magnetization inside Ω_1 is denoted by $\mathbf{m_1}$ and outside it by $\mathbf{m_2}=(1,0)$. The unit vector normal to the wall C is designated by $\mathbf{n}_C$. Applying the Gauss theorem to the first quadrant, we obtain

$$\int_{\Omega_1} \nabla \cdot \mathbf{M} d\boldsymbol{\rho} + \int_C M_s(\mathbf{m_1}-\mathbf{m_2})\cdot \mathbf{n}_C dl = -M_s R. \quad (4)$$

Developing the first term of the left side of Eq. (4) we reach

$$\eta_w - \int_C \mathbf{m_2}\cdot\mathbf{n}_C dl - \int_{\eta=\eta_w} \mathbf{m_1}\cdot\mathbf{n}_\eta dl = 0, \quad (5)$$

where $\mathbf{n}_\eta=(0,1)$ is the unit vector normal to the straight line $\eta=\eta_w$. Thus, once fixed the function $\eta=f(\xi)$, which defines the wall, Eq. (5) gives the point (ξ_w, η_w) that belongs to $\eta=f(\xi)$, and that makes it satisfy the Gauss theorem. The position of this point can be taken as the characteristic size of the closure pattern, i.e., of the confinement distance L of the $-1/2$ singularities induced by the hole.

In order to find the function $\eta=f(\xi)$ that defines the wall, we evaluated Eq. (5) for different expressions. For straight walls, for example, as depicted in the sketch of Fig. 6, the conditions imposed by charge conservation cannot be fulfilled. The only expressions for which there exists a point (ξ_w, η_w) that meets the Gauss theorem are paraboliclike functions with an asymptote perpendicular to the easy axis of anisotropy. Also, in order to match the results of the MFM observations and micromagnetic simulations, shown in Figs. 2 and 3, two extra restrictions must be verified: first, all the magnetic charges in Ω_1 must have the same sign, i.e., the function $\eta=f(\xi)$ should depart from point (1,0) above the boundary between the region that separates positive and negative charges; second, the linear charge density on the wall should be always of the same sign and decrease gradually from the point (1,0) to a point denoted by (ξ_0, η_0), in which the charge density on the wall becomes zero. A reasonable set of trial functions can be given by the vertical branch of the right strophoid with pole in point (1,0) and a vertical asymptote at a distance a from the mentioned pole [see Fig. 7(a)],

$$\eta^2 = (\xi-1)^2\left(\frac{a+\xi-1}{a-\xi+1}\right). \quad (6)$$

This kind of walls fulfills all the above requirements: they bound a Ω_1 region with only negative charges, there is always a point (ξ_w, η_w) which meets the Gauss theorem, and the charge density of the wall is always of the same sign, decreasing monotonically from a maximum value at the point (1,0) to zero at the point (ξ_0, η_0). Even more, this point (ξ_0, η_0) matches the one numerically obtained from Eq. (5): (ξ_w, η_w). Thus the wall terminates smoothly at the point determined by the Gauss theorem [see Fig. 7(b) for the charge density on a wall given by Eq. (6) with $a=1$; the point $\xi_w=1.94$, which verifies the Gauss theorem for $a=1$, has also been depicted]. For this kind of walls, the ratio η_w/ξ_w, which is a measure of the geometrical shape of the closure configuration, is close to unity for small values of η_w and increases up to almost 3 as the size of the closure structure increases in a similar way as the behavior obtained in the micromagnetic calculations for the ratio L_y/L_x.

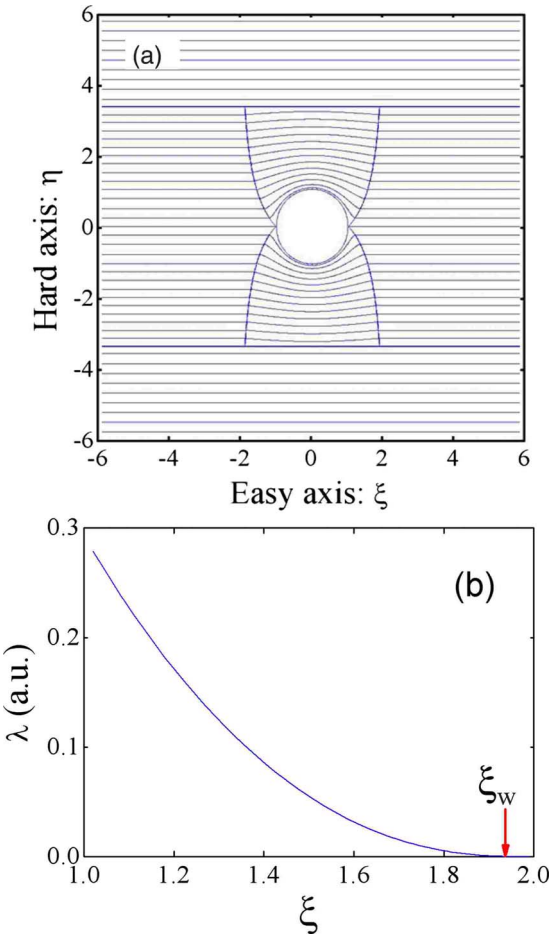

FIG. 7. (Color online) (a) Closure domain structure around the hole with walls described by Eq. (6) with $a=1$. (b) Linear density of magnetic charges λ along the wall calculated for $a=1$. Arrow indicates the point ξ_w at which Gauss theorem is satisfied.

The previous results suggest that the function given by Eq. (6) adequately represents the walls that appear in the systems under study. But Eq. (6) does not define a single wall, it defines a uniparametric family of walls—one for each parameter value a. For every wall of the family, there is only one point (ξ_w, η_w) that moves away from the hole as a increases with a linear dependence of η_w on a. From this family of walls only the one that minimizes the total energy

will be adopted by the system. Therefore, in order to determine the equilibrium configuration of the system, we must compute the total energy and minimize it with respect to parameter a.

The total energy is the sum of two terms: magnetostatic energy E_m and anisotropy energy E_K. The magnetostatic energy arises from the interaction between the magnetic charges that were generated on the surface and on the walls. The magnetization distribution leads to a surface charge density $\sigma(\boldsymbol{\rho})=-M_s[\nabla\cdot\mathbf{m}(\boldsymbol{\rho})]$ which is negative in the first and fourth quadrants and positive in the second and third quadrants. On the walls, there will be a linear density $\lambda(\boldsymbol{\rho})=M_s(\mathbf{m_1}-\mathbf{m_2})\cdot\mathbf{n}_C$ which is positive in the walls of the first and fourth quadrants and negative in the walls of the second and third quadrants. Hence, the magnetostatic energy of the system is given by

$$E_m = E_s + \sum_{i=1}^{4} E_{is} + \sum_{i,j} E_{ij}, \tag{7}$$

where E_s is the term for the interaction between the surface charges, E_{is} is for the interaction between the wall i and the surface charges, and E_{ij} is for the interaction between the walls i and j. The complex mixture of magnetic charges given by the closure structure of Fig. 7(a) greatly reduces the total magnetostatic energy and is very different from the closure structures around holes in bulk materials that simply dilute the charges in a larger volume keeping the dipolar character. It might be related with the longer range of the potential created by the charges that is logarithmic in 2D (Refs. 37 and 38) as compared to $1/r$ in 3D. Thus, the previously defined magnetostatic energies are given by the following expressions:

$$E_s = -\frac{\mu_o M_s^2}{4\pi}\int_\Omega\int_\Omega [\nabla\cdot\mathbf{m}(\boldsymbol{\rho})][\nabla\cdot\mathbf{m}(\boldsymbol{\rho}')]\ln(|\boldsymbol{\rho}-\boldsymbol{\rho}'|)d^2\rho d^2\rho', \tag{8}$$

$$E_{is} = -\frac{\mu_o M_s^2}{2\pi}\int_\Omega\int_C [\nabla\cdot\mathbf{m}(\boldsymbol{\rho})]\{[\mathbf{m_1}(\boldsymbol{\rho}')-\mathbf{m_2}(\boldsymbol{\rho}')]\cdot\mathbf{n}_C(\boldsymbol{\rho}')\}\ln(|\boldsymbol{\rho}-\boldsymbol{\rho}'|)d^2\rho dl', \tag{9}$$

$$E_{ij} = -\frac{\mu_o M_s^2}{2\pi}\int_C\int_{C'} \{[\mathbf{m_1}(\boldsymbol{\rho})-\mathbf{m_2}(\boldsymbol{\rho})]\cdot\mathbf{n_C}(\boldsymbol{\rho})\}\times\{[\mathbf{m_1}(\boldsymbol{\rho}')-\mathbf{m_2}(\boldsymbol{\rho}')]\cdot\mathbf{n}_{C'}(\boldsymbol{\rho}')\}\ln(|\boldsymbol{\rho}-\boldsymbol{\rho}'|)dldl'. \tag{10}$$

The anisotropy energy is

$$E_K = K\int_\Omega \{1-[\mathbf{m}(\boldsymbol{\rho})\cdot\mathbf{e}]^2\}\,d^2\rho \tag{11}$$

and the total energy can be written as

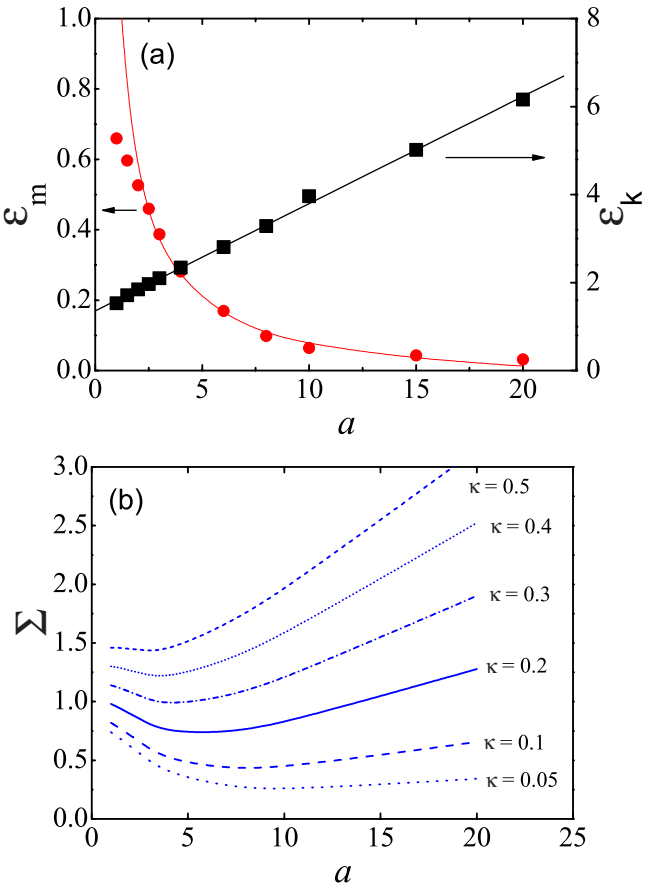

FIG. 8. (Color online) (a) Normalized magnetostatic energy ε_m (circles) and normalized anisotropy energy ε_k (squares) as a function of domain-wall parameter a. Dashed line is a fit to $1/a$ dependence and solid line is a linear fit. (b) Total system energy vs a for different values of κ. Note that the minima in the curves are displaced to larger values of a as κ decreases.

$$E = -\frac{\mu_o M_s^2}{2\pi}\left[\frac{1}{2}\varepsilon_s + \sum_i \varepsilon_{is} + \sum_{ij}\varepsilon_{ij}\right] + K\varepsilon_k \tag{12}$$

representing ε_s, ε_{is}, ε_{ij}, and ε_k the integrals appearing in Eqs. (8)–(11), respectively. This result can be normalized as follows:

$$\Sigma \equiv \frac{2E}{\mu_o M_s^2} = -\frac{1}{\pi}\left[\frac{1}{2}\varepsilon_s + \sum_i \varepsilon_{is} + \sum_{ij}\varepsilon_{ij}\right] + \kappa\varepsilon_k, \tag{13}$$

where $\kappa \equiv 2K/\mu_0 M_s^2$.

Figure 8(a) shows the numerical results obtained for the normalized magnetostatic energy $\varepsilon_m = 2E_m/\mu_0 M_s^2$ (circles) and normalized anisotropy energy ε_k (squares) as a function of the parameter a that determines wall shape. ε_m follows approximately a $1/a$ dependence (dotted line), whereas ε_k increases linearly with a (solid line). Figure 8(b) shows the total energy Σ vs a calculated from Eq. (13) for different values of the reduced anisotropy κ. All the curves show a minimum, corresponding to the stable system configuration, that moves toward longer distances as κ decreases. Considering the approximate analytical dependencies of ε_m and ε_k

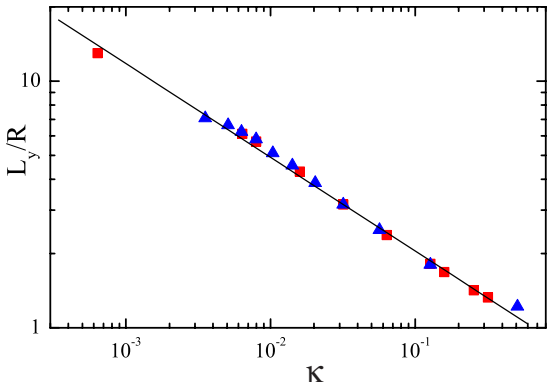

FIG. 9. (Color online) κ dependence of the size of the closure structure along the hard axis obtained from micromagnetic simulations: triangles varying M_s ($K=8\times10^2$ J/m^3, $A=1\times10^{-11}$ J/m) and squares varying K ($M_s=2\times10^5$ A/m, $A=1\times10^{-11}$ J/m). Solid line corresponds to a $L_y\sim\kappa^{-0.4}$ dependence.

on a, this optimum value of a that defines the characteristic length scale of the closure structure around the hole should scale as $a\sim\kappa^{-0.5}$. Taking into account the linear dependence of confinement distance along the hard axis η_w on a, we might compare these predictions with the results of the micromagnetic simulations for L_y, which is the size of the closure structure perpendicular to the easy axis. Figure 9 shows L_y/R vs κ derived from the OOMMF simulations as a function of M_s (triangles) and K (squares). All the points coalesce on a single line, confirming that κ is indeed the relevant physical parameter that determines the size of the closure structure. This dependence can be described by a power law of the form $L_y\sim\kappa^{-0.4}$ (solid line), indicating a stronger confinement of the $-1/2$ defects close to the hole as the reduced anisotropy increases. We might compare the obtained behavior with other micromagnetic structures in thin films that are also determined by the interplay between magnetostatic and anisotropy energies such as the width of a Néel wall tail[28] that scales as $W_{\text{tail}}\sim\kappa^{-1}$. The different κ dependence found in the present case can be attributed mainly to the differences between the magnetic charge distribution that appears around the hole and that of a Néel wall in which the film is simply divided in two oppositely charged regions. Thus, the weight of the contribution of the magnetostatic term in the global energy balance should be smaller for the studied closure structure than for a Néel wall, allowing for a stronger confinement of the closure structure (i.e., a weaker κ dependence taking into account the inverse proportionality between κ and M_s^2).

VI. CONCLUSIONS

In summary, the closure domain structure around a single hole in a uniaxial magnetic thin film can be described as two $-1/2$ half vortices located at opposite sides of the hole along the anisotropy easy axis and confined within a distance L. It appears as two sets of charged Néel walls emanating from the singularity points that bound two regions in which the magnetization curves around the hole and gives rise to a distribution of magnetic charges at the film surface. The confinement distance L is determined by the interplay between magnetostatic and anisotropy energies, constrained by the conservation of magnetic charges within the system. It scales approximately as $L_y\sim\kappa^{-0.4}$, which is a relatively weak dependence that is probably related with the mixture of magnetic charges around the hole that reduces the weight of the magnetostatic term in the global energy balance.

ACKNOWLEDGMENTS

This work was supported by Spanish Ministerio de Educacion y Ciencia under Grants No. NAN2004-09087, No. FIS2005-07392, and No. FIS2008-06249. G.R.R acknowledges financial support from I3P grants program and MERG-CT-2004-513625.

*jmartin@condmat.uniovi.es

[1] For a review, see J. I. Martín, J. Nogués, K. Liu, J. L. Vicent, and I. K. Schuller, J. Magn. Magn. Mater. **256**, 449 (2003).
[2] S. S. P. Parkin, M. Hayashi, and L. Thomas, Science **320**, 190 (2008).
[3] J. Rothman, M. Kläui, L. Lopez-Díaz, C. A. F. Vaz, A. Bleloch, J. A. C. Bland, Z. Cui, and R. Speaks, Phys. Rev. Lett. **86**, 1098 (2001).
[4] S. P. Li, D. Peyrade, M. Natali, A. Lebib, Y. Chen, U. Ebels, L. D. Buda, and K. Ounadjela, Phys. Rev. Lett. **86**, 1102 (2001).
[5] F. J. Castaño, C. A. Ross, A. Eilez, W. Jung, and C. Frandsen, Phys. Rev. B **69**, 144421 (2004).
[6] F. Q. Zhu, G. W. Chern, O. Tchernyshyov, X. C. Zhu, J. G. Zhu, and C. L. Chien, Phys. Rev. Lett. **96**, 027205 (2006).
[7] R. P. Cowburn, A. O. Adeyeye, and J. A. C. Bland, Appl. Phys. Lett. **70**, 2309 (1997).
[8] P. Vavassori, G. Gubiotti, G. Zangari, C. T. Yu, H. Yin, H. Jiang, and G. J. Mankey, J. Appl. Phys. **91**, 7992 (2002).
[9] I. Ruiz-Feal, L. Lopez-Díaz, A. Hirohata, J. Rothman, C. M. Guertler, J. A. C. Bland, L. M. García, J. M. Torres, J. Bartolomé, F. Bartolomé, M. Natali, D. Decanini, and Y. Chen, J. Magn. Magn. Mater. **242-245**, 597 (2002).
[10] Z. L. Xiao, C. Y. Han, U. Welp, H. H. Wang, V. K. Vlasko-Vlasov, W. K. Kwok, D. J. Miller, J. M. Hiller, R. E. Cook, G. A. Willing, and G. W. Crabtree, Appl. Phys. Lett. **81**, 2869 (2002).
[11] T. A. Moore, G. Wastlbauer, J. A. C. Bland, E. Cambril, M. Natali, D. Decanini, and Y. Chen, J. Appl. Phys. **93**, 8746 (2003).
[12] A. Pérez-Junquera, V. I. Marconi, A. B. Kolton, L. M. Álvarez-Prado, Y. Souche, A. Alija, M. Vélez, J. V. Anguita, J. M. Alameda, J. I. Martín, and J. M. R. Parrondo, Phys. Rev. Lett. **100**, 037203 (2008).
[13] M. Rahm, J. Stahl, and D. Weiss, Appl. Phys. Lett. **87**, 182107 (2005).
[14] M. Beleggia, J. W. Lau, M. A. Schofield, Y. Zhu, S. Tandon, and

M. De Grae, J. Magn. Magn. Mater. **301**, 131 (2006).
[15] L. Torres, L. Lopez-Díaz, and J. Iñiguez, Appl. Phys. Lett. **73**, 3766 (1998).
[16] O. Tchernyshyov and G. W. Chern, Phys. Rev. Lett. **95**, 197204 (2005).
[17] L. Neel, Cah. Phys. **21**, 25 (1944).
[18] L. J. Dijkstra and C. Pert, Phys. Rev. **79**, 979 (1950).
[19] E. Della Torre and M. Torfeh-Isfahani, J. Appl. Phys. **53**, 4309 (1982).
[20] S. Chikazumi, *Physics of Magnetism* (Krieger, Malabar, 1978).
[21] S. Methfessel, S. Middelhoek, and H. Thomas, IBM J. Res. Dev. **4**, 96 (1960); G. A. Jones, Br. J. Appl. Phys. **15**, 857 (1964).
[22] L. Lopez-Díaz and E. Della Torre, J. Appl. Phys. **83**, 5933 (1998).
[23] C. Merton, G. D. Skidmore, J. Schmidt, E. D. Dahlberg, H. Wan, and B. Pant, J. Appl. Phys. **85**, 4601 (1999).
[24] A. Pérez-Junquera, G. Rodríguez-Rodríguez, M. Vélez, J. I. Martín, H. Rubio, and J. M. Alameda, J. Appl. Phys. **99**, 033902 (2006).
[25] H. A. M. van den Berg, J. Appl. Phys. **57**, 2168 (1985); **60**, 1104 (1986); **62**, 1952 (1987).
[26] P. Bryant and H. Suhl, Appl. Phys. Lett. **54**, 78 (1989).
[27] G. Bertotti, *Hysteresis in Magnetism* (Academic, San Diego, 1998), p. 204.
[28] A. Huber and R. Schäfer, *Magnetic Domains* (Springer, Berlin, 1998).
[29] M. J. Donahue and D. G. Porter, "OOMMF User's Guide, Version 1.0," National Institute of Standards and Technology Interagency Report NISTIR 6376, 1999; Object Oriented Micromagnetic Framework is available at http://math.nist.gov/oommf
[30] A. Pérez-Junquera, J. I. Martín, M. Vélez, J. M. Alameda, J. V. Anguita, F. Briones, E. M. González, and J. L. Vicent, Nanotechnology **15**, S131 (2004).
[31] G. Rodríguez-Rodríguez, A. Pérez-Junquera, M. Vélez, J. V. Anguita, J. I. Martín, H. Rubio, and J. M. Alameda, J. Phys. D **40**, 3051 (2007).
[32] M. Barthelmess, C. Pels, A. Thieme, and G. Meier, J. Appl. Phys. **95**, 5641 (2004); C. T. Hsieh, J. Q. Liu, and J. T. Lue, Appl. Surf. Sci. **252**, 1899 (2005).
[33] K. Metlov, Appl. Phys. Lett. **79**, 2609 (2001).
[34] S. Huo, G. Pan, D. J. Mapps, W. W. Clegg, G. Heydon, W. M. Rainforth, H. A. Davies, J. E. L. Bichop, J. W. Tucker, and M. R. J. Gibbs, J. Appl. Phys. **87**, 1096 (2000).
[35] S. McVitie, G. S. White, J. Scott, P. Warin, and J. N. Chapman, J. Appl. Phys. **90**, 5220 (2001); J. M. Garcia, A. Thiaville, and J. Miltat, J. Magn. Magn. Mater. **249**, 163 (2002).
[36] A. D. Polyanin, *Handbook of Linear Partial Differential Equations for Engineers and Scientists* (Chapman and Hall, London/CRC, Boca Raton, 2004).
[37] P. M. Morse and H. Feshbach, *Methods of Theoretical Physics* (McGraw-Hill, New York, 1953).
[38] E. Durand, *Electrostatique, Tome I: Les distributions.* (Masson, Paris, 1964).